PERGAMON

International Journal of Solids and Structures 40 (2003) 2421–2448

INTERNATIONAL JOURNAL OF SOLIDS and STRUCTURES

www.elsevier.com/locate/ijsolstr

A spectrally formulated finite element for wave propagation analysis in functionally graded beams

A. Chakraborty, S. Gopalakrishnan *

Department of Aerospace Engineering, Indian Institute of Science, Bangalore 560012, India

Received 13 June 2002; received in revised form 21 November 2002

Abstract

In this paper, spectral finite element method is employed to analyse the wave propagation behavior in a functionally graded (FG) beam subjected to high frequency impulse loading, which can be either thermal or mechanical. A new spectrally formulated element that has three degrees of freedom per node (based upon the first order shear deformation theory) is developed, which has an exact dynamic stiffness matrix, obtained by exactly solving the homogeneous part of the governing equations in the frequency domain. The element takes into account the variation of thermal and mechanical properties along its depth, which can be modeled either by explicit distribution law like the power law and the exponential law or by rule of mixture as used in composite. Ability of the element in capturing the essential wave propagation behavior other than predicting the propagating shear mode (which appears only at high frequency and is present only in higher order beam theories), is demonstrated. Propagation of stress wave and smoothing of depthwise stress distribution with time is presented. Dependence of cut-off frequency and maximum stress gradient on material properties and FG material (FGM) content is studied. The results are compared with the 2D plane stress FE and 1D Beam FE formulation. The versatility of the method is further demonstrated through the response of FG beam due to short duration highly transient temperature loading.

Keywords: Functionally graded materials; Thermal loading; Stress pattern; Wave propagation; High frequency; Spectral element method; Wave number; Dispersion relation

---

1. Introduction

An ideal material combines the best properties of metals and ceramics—the toughness, electrical conductivity, and machinability of metals, and the low density, high strength, high stiffness, and temperature resistance of ceramics. In recent years, these type of advanced materials are no longer dreams but properly conceived and developed. These materials are known as metal matrix composites (MMCs) or ceramic matrix composites (CMCs) and they have incredible promise in many engineering applications. Demand

---

* Corresponding author. Tel.: +91-080-309-2757; fax: +91-080-360-0134.
E-mail address: krishnan@aero.iisc.ernet.in (S. Gopalakrishnan).

doi:10.1016/S0020-7683(03)00029-5

for such materials comes from the automotive industry (lightweight and strong materials would increase fuel efficiency and last longer), electronics, telecommunications, and the aerospace and defense industries. The gradation in properties of the material reduces the thermal stresses, the residual stresses, and the stress concentration factors. If two dissimilar materials are bonded together, there is a very high chance that debonding will occur at some extreme loading conditions, be it static, dynamic, or thermal load. Cracks are likely to initiate at interfaces and grow into the weaker material section. Another problem associated with such structures is the presence of residual stresses due to the difference in coefficients of thermal expansion between the materials of adjacent layers. By gradually varying the volume fraction of the constituents rather than abruptly changing them over an interface can resolve these problems. The gradual variation results in a very efficient material tailored to suit the needs.

Advanced materials can be "functionally graded" to provide the ideal combination of characteristics desired. FGMs are materials in which the material properties vary with location in such a way as to optimize some function of the overall FGM. The matrix alloy (the metal), the reinforcement material (the ceramic), the volume, shape, and location of the reinforcement, and the fabrication method can all be tailored to achieve particular desired properties. In MMCs, for example, ceramic reinforcements in the form of either fibers, whiskers, or particulates are introduced into the metal; the structure is controlled at scales varying from 100 nm to several millimeters.

FGM has gained widespread applicability as thermal-barrier structures, wear and corrosion resistant coatings, and they are also used for joining dissimilar materials (Suresh and Mortensen, 1998). FGMs consisting of metallic and ceramic components are well known to improve the properties of thermal-barrier systems, caused because of cracking or delamination. These are often observed in the conventional two-layer systems, which are avoided by the smooth transition between the properties of the components in FGMs. In defense applications, for example, faster transportation of armor is necessary. The fundamental problem that limits its applicability is the weight of the armor. That is, the weight of materials inhibit fast movement and incur heavy consumption of fuel. MMCs have received considerable attention to alleviate this problem due to their lightness and ability to work harden under dynamic loading. However, damage to the armor from shockwaves can limit the work hardening. An FGM can be used here to tailor the microstructure of the MMC. A typical modern composite armor consists a hard outer surface, typically an Al_2O_3 tile, backed by a ductile material such as aluminium. These type of combinations, in impact environment, are often subjected to tensile wave, generated because of the reflection at the interface between the hard and ductile material due to acoustic impedance mismatch. This is of great concern because ceramic materials typically have low tensile strengths. FGM can be used here to diffuse the reflection by smoothly varying the properties from ceramic to metal.

In another application of FGM, thin walled members like plates and shells, which are used in reactor vessels, turbines and other machine parts, are susceptible to failure from buckling, large amplitude deflections, or excessive stresses induced by thermal or combined thermo-mechanical loading. Functionally gradient coatings on these structural elements may help reduce the failures.

Analysis of FGM involves consideration of temperature change, which imparts thermal loading of significant amount due to mismatch in thermal coefficients between metallic and ceramic materials. Reddy and Chin (1998) have already dealt with this problems for static and transient loading. El-Abbasi and Meguid (2000) analysed the thermoelastic behavior of functionally graded plates and shells. In this work, explicit coupling of thermal and mechanical field is not considered. Only the external thermal effect in the form of strain is considered. Power law and exponential variation of the material properties through the depth of the beam are considered in this study.

One of the fundamental characteristics of the wave propagation problem is that the incident pulse duration is very small (of the order of micro seconds) and hence the frequency content of pulse is very high (of the order of kHz). When such a pulse is applied to the structure, it will force all the higher order modes to participate in the response. At higher frequencies, the wave lengths are small. Hence, in order to capture all the higher order modes, the conventional finite element method requires very fine mesh to match the wavelengths. This makes the system size enormously large.

The spectral element approach (SEA) could be the nice alternative for such problems (Doyle, 1999). In SEA, first the governing equation is transformed in frequency domain using discrete Fourier transform (DFT). In doing so, for 1D waveguides, the governing partial differential equation (PDE) is reduced to a set of ordinary differential equation's (ODE) with constant coefficients, with frequency as a parameter. The resulting ODEs are much easier to solve than the original PDE. The SEA begins with the use of exact solution to governing ODEs in the frequency domain as interpolating function. The use of exact solution results in exact mass distribution and hence the resulting dynamic stiffness matrix is exact. Hence, in the absence of any discontinuity, one single element is sufficient to handle a beam of any length. This substantially reduces the system size and they are many order smaller than the sizes involved in the conventional FEM. First, the exact dynamic stiffness is used to determine the system transfer function (frequency response function). This is then convolved with load. Next, inverse fast Fourier transform (IFFT) is used to get the time history of the response. Spectral element for elementary rod (Doyle, 1988), elementary beam (Doyle and Farris, 1990a,b), Timoshenko beam (Gopalakrishnan et al., 1992), for higher order Mindlin Hermann rod (Martin et al., 1994), for elementary composite beam (Roy Mahapatra et al., 2000) and for 2D membrane element (Rizzi and Doyle, 1991) are reported in literature. Till date, to the best of authors' knowledge no spectral finite element formulation is available in the literature for FGM beams.

In addition to the smaller system sizes, there are many advantages that are inherent to the SEA. These are summarized below: (1) Treatment of non-reflecting boundary conditions are simple and straight-forward. This is done by leaving out the terms associated with the reflected coefficients from the interpolating displacement functions. Such an element is called the "Throw-off" element and it amounts to adding maximum damping to the structure. (2) Since the system transfer function is direct by product of the approach, performing inverse problems, such as, system identification and force identification, is straight forward. (3) The method is easily amenable for control related problem. A novel active spectral element (Roy Mahapatra et al., 2001) was formulated for this purpose. This has great utility in smart structure research for noise and vibration suppression.

Wave propagation analysis of FGM beam poses tremendous challenge due to the presence of material anisotropy. Because of this, an additional shear wave gets created beyond a certain high frequency, called the cut-off frequency. Due to this, there will be a three way (axial shear bending) coupling of modes. Tracking these individual waves is a very difficult task specially for a dispersive system such as a FGM beam. In this work, we have devised an efficient methodology to capture such coupled waves.

The literature on the response of such advanced materials to dynamic and impact loadings (severe mechanical environments) are limited in numbers. No results existed for the case of through-thickness material property varying plates using shear deformation plate theories with the von Kármán non-linearity until the works of Reddy and Chin (1998), Praveen and Reddy (1998) and Reddy (2000) appeared. Non-linear transient thermoelastic analysis of FGM was carried out in Reddy and Chin (1998) by plate finite element for moderately large rotations (i.e., the von-Kármán non-linear theory of plates). Gong et al. (1999) studied the elastic response of FGM shell subjected to low velocity impact. The existing literature on the responses of FGM to high frequency impact loading are very limited in numbers. Among them, there are only methods proposed to analyse wave propagation problems in FGM plates. Liu et al. (1991a,b) and Liu and Tani (1992, 1994), used strip element method for FGM plates. An analytical method was proposed by Ohyoshi et al. (1996), where the wave reflection and the transmission coefficients were obtained for FGM plate. Thermomechanical behavior of FGM plates and shells was investigated by Reddy and Chin (1998). Non-linear transient thermoelastic analysis of FGM was carried out by Praveen and Reddy (1998) using plate finite element for moderately large rotation in von-Kármán sense. Liu et al. (1999) proposed a method for analysing stress waves in FGM plates, where it is shown that the variation of material properties can be approximated by a piecewise linear function. Recently, Han et al. (2002a) presented an analytical–numerical method for analysing characteristics of waves in a cylinder composed of FGM. They have also proposed a numerical method for analysing transient waves in plates of FGM excited by impact loads (Han et al., 2002b). Here, the displacement response is determined by employing Fourier transformation and the modal analysis.

Till date, the only work involving wave propagation in FGM beam is that of Chakraborty et al. (2002), where an exact finite element is developed which takes thermal strain and depthwise property variation into consideration.

The organization of the paper is as follows. In the next two sections, the details of the formulation of the spectral element is given. Next, the numerical studies are performed. First, the predicting capability of the element is tested by observing the normal wave propagation behavior and the result is compared with the 2D finite element (FE) solution. Second, the stress wave propagation through FG beam and the variation of stress with depth and the smoothening effect of FGM is inspected closely. Effect of thermal loading is investigated next. Here, a thermal burst kind of loading is applied to the beam structure and its response is observed. Lastly, the presence of bending-axial-shear coupling in FG beam is demonstrated. Based on the results, a number of important conclusions are drawn.

2. Mathematical model

Considering the first order shear deformation theory, the axial and transverse displacement field can be expressed as

$$U(x,y,z,t) = u^{\circ}(x,t) - z\phi(x,t), \qquad W(x,y,z,t) = w^{\circ}(x,t), \tag{1}$$

where u° and w° are the mid-plane axial and transverse displacements in the reference plane respectively and ϕ is rotation about Y axis (see Fig. 2(a)) and z is measured from the reference plane. Using Eq. (1) and adding the strain due to temperature, the normal and shear strains can be written as

$$\epsilon_{xx} = u^{\circ}_{,x} - z\phi_{,x} - \alpha(z)\Delta T(x), \qquad \gamma_{xz} = -\phi + w^{\circ}_{,x}. \tag{2}$$

Here $(.)_{,x}$ represents differentiation with respect to x. $\alpha(z)$ is the coefficient of thermal expansion of the FGM material, which varies along depth and ΔT is the temperature change to which the beam is subjected and in general can vary along the length. The constitutive relation for FGM is given by

$$\sigma_{xx} = E(z)\varepsilon_{xx}, \qquad \tau_{xz} = G(z)\gamma_{xz}, \tag{3}$$

where σ_{xx} and ε_{xx}, are normal stresses and normal strains in the x direction and τ_{xz} and γ_{xz} are shear stress and shear strain in the x–z plane. $E(z)$ and $G(z)$ are Young's modulus and Shear modulus, which vary with depth z.

It can be assumed that material properties are varying according to some well-defined rule like the exponential law and the power law. The exponential law is given by,

$$\mathscr{P}(z) = \mathscr{P}_t \exp(-\delta(1 - 2z/h)), \quad \delta = \frac{1}{2}\log\left(\frac{\mathscr{P}_t}{\mathscr{P}_b}\right) \tag{4}$$

and the power law (for Voight type estimate (Markworth et al., 1995)) is given by

$$\mathscr{P}(z) = (\mathscr{P}_t - \mathscr{P}_b)\left(\frac{z}{h} + \frac{1}{2}\right)^n + \mathscr{P}_b, \tag{5}$$

where $\mathscr{P}(z)$ denotes a typical material property (E, G, α, ϱ). $\mathscr{P}_t$ and $\mathscr{P}_b$ denote property values of the variables at topmost and bottommost layer of the beam, respectively and n is an exponent whose value ranges from 1 to 5. h is the thickness of FGM layer whose mid-plane has coordinate $z = 0$.

Another way of estimating material properties is the rule of mixture which is generally employed in composite materials. Summary of this method can be found in Tsai and Hahn (1980) and Jones (1975). The concept of equivalent homogeneity yields composite sphere model, three phase model, composite cylinder model and self consistent scheme (Christensen, 1979). Composite sphere and cylinder models can be further improved by the step-by-step (SBS) method as given in Liu (1998). The method given for particle reinforced composite material is best suited for use in present context. The details are omitted here. In short, FGM can be treated as a matrix-particle mixture of different particle volume fraction which is smoothly varied along the beam depth. The two different materials at the top and bottom of the beam play the role of the matrix and the particle.

These different models for material property variation is compared in Fig. 1, where the variation of Young's modulus along depth is plotted. Top and bottom materials (particle and matrix, respectively for SBS method) are taken as steel and ceramic with Young's modulus ratio 1.857. The figure clearly shows different trends of distribution for different models. In the SBS method 'constant area composition' is used and particle volume fraction V_{p1}, is taken as 0.001. Since, the SBS method predicts only the elastic and thermal properties, in subsequent calculations where SBS method is used, the inertial properties are evaluated by the power law model with suitable value of the exponent n.

Applying Hamilton's principle, the following differential equations of motions are obtained in terms of the three degrees of freedom (u°, w° and ϕ):

$$\delta u: \quad I_\circ \ddot{u}^\circ - I_1\ddot{\phi} - A_{11}u^\circ_{,xx} + B_{11}\phi_{,xx} + AT_{11}\Delta T_{,x} = 0, \tag{6}$$

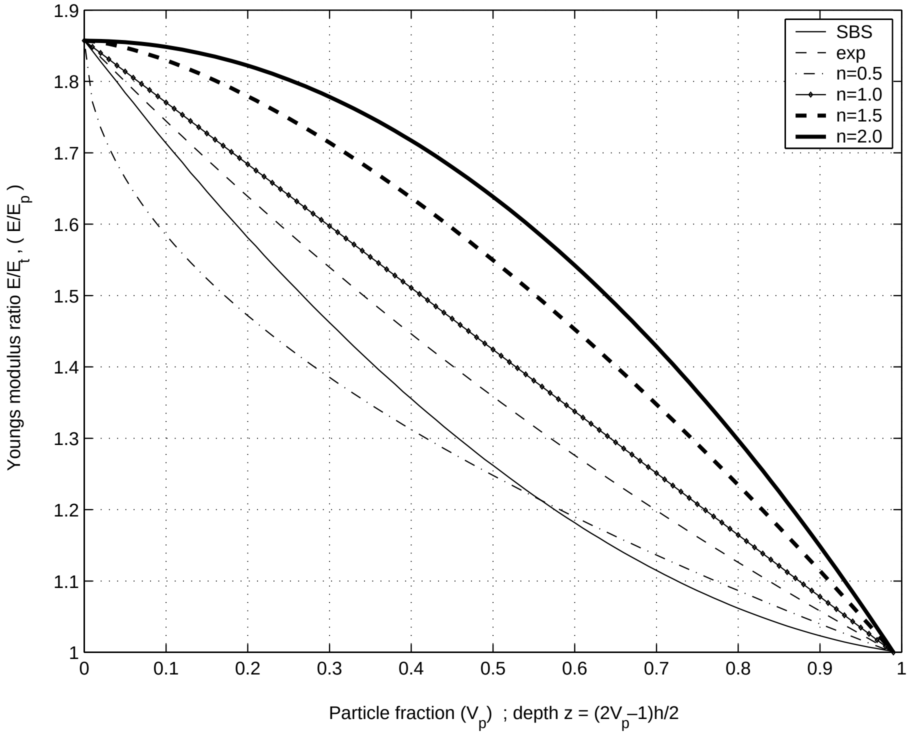

Fig. 1. Variation of Young's modulus for different model.

$$\delta w^\circ : \quad I_\circ \ddot{w}^\circ - A_{55}(w^\circ_{,xx} - \phi_x) = 0, \tag{7}$$

$$\delta \phi : \quad I_2 \ddot{\phi} - I_1 \ddot{u}^\circ + B_{11} u^\circ_{,xx} - D_{11}\phi_{,xx} - A_{55}(w^\circ_{,x} - \phi) - BT_{11}\Delta T_{,x} = 0 \tag{8}$$

and associated force boundary equations can be expressed as

$$A_{11}u^\circ_{,x} - B_{11}\phi_{,x} - AT_{11}\Delta T(x) = N_x, \tag{9}$$

$$A_{55}(w^\circ_{,x} - \phi) = V_x, \quad -B_{11}u^\circ_{,x} + D_{11}\phi_{,x} + BT_{11}\Delta T(x) = M_x, \tag{10}$$

where N_x, V_x and M_x denote axial force, shear force and bending moment at any boundary point $x = 0$ or $x = L$. The stiffness coefficients and the mass moments are obtained as

$$[A_{11}\ B_{11}\ D_{11}] = \int_A E(z)[1\ \ z\ \ z^2]\,\mathrm{d}A, \qquad A_{55} = \int_A G(z)\,\mathrm{d}A, \tag{11}$$

$$[AT_{11}\ BT_{11}] = \int_A E(z)\alpha(z)[1\ \ z]\,\mathrm{d}A, \qquad [I_0\ I_1\ I_2] = \int_A \varrho(z)[1\ \ z\ \ z^2]\,\mathrm{d}A. \tag{12}$$

The governing differential equations (6)–(8) represent a system of coupled linear hyperbolic non-homogeneous PDE, which is difficult to solve exactly in the time domain for all boundary conditions. The spectral method begins by transforming the field variables (here displacements) to the frequency domain using discrete Fourier transform (DFT) and substituting them in the homogeneous form of the governing PDE. The discretized spectral form of the displacement field is expressed as

$$\mathbf{u}(x,t) = \sum_n^N \hat{\mathbf{u}}(x,\omega_n)\,\mathrm{e}^{\mathrm{i}\omega_n t} = \sum_n^N \left(\sum_j^{n_j} (\tilde{\mathbf{u}}_j \mathrm{e}^{-\mathrm{i}k_j x}) \right) \mathrm{e}^{\mathrm{i}\omega_n t}, \tag{13}$$

where $\mathrm{i} = \sqrt{-1}$, ω_n is the frequency at nth sampling point and k_j is the wave number associated with the jth mode of propagation (forward or backward) at ω_n. N is the Nyquist frequency in FFT used for computer implementation. $\hat{\mathbf{u}} = \{\hat{u}\,\hat{w}\,\hat{\phi}\}^T$ denotes the spectral amplitude vector corresponding to the generic displacement vector as a function of (x,ω_n). $\tilde{\mathbf{u}}_j = \{\bar{u}_j\,\bar{w}_j\,\bar{\phi}_j\}^T$ represents the wave coefficient vector associated with jth mode of propagation at frequency ω_n. n_j is the number of propagating modes (6 for this model, 3 forward and 3 backward moving waves). Substituting the field variables in homogeneous form of Eq. (6)–(8), in terms of wave coefficients in Eq. (13), we get the characteristic equation as

$$\begin{bmatrix} (k_j^2 - k_a^2) & 0 & \left(s_1 s_2 k_a^2/k_r - r k_a k_j^2/k_r^2\right) \\ 0 & (k_j^2 - k_r^2) & -\mathrm{i}k_j \\ \left(r k_r^2 k_j^2/k_a k_b^2 - s_1 s_2 k_r\right) & -\mathrm{i}k_j & \left(s_1^2 - 1 - k_r^2 k_j^2/k_b^4\right) \end{bmatrix} \begin{Bmatrix} \bar{u}_j \\ \bar{v}_j \\ \bar{w}_j \end{Bmatrix} = \mathbf{0}, \tag{14}$$

where k_a, k_b and k_r are the wave numbers of uncoupled axial, flexural and shear wave modes respectively. They are defined as the ratio of frequency and corresponding phase speeds and can be expressed as

$$k_a = \omega_n/c_a, \quad k_b = \omega_n/c_b, \quad k_r = \omega_n/c_r, \tag{15}$$

$$c_a = \sqrt{A_{11}/I_\circ}, \quad c_b = \sqrt[4]{D_{11}\omega_n^2/I_\circ}, \quad c_r = \sqrt{A_{55}/I_\circ}. \tag{16}$$

In Eq. (14), r and s_2 are the non-dimensional axial-flexural coupling parameters due to stiffness and material asymmetry respectively. s_1 is non-dimensional flexural-shear coupling parameter. They are given by

$$r = \sqrt{B_{11}^2/(A_{11}D_{11})}, \quad s_1 = \omega_n\sqrt{I_2/A_{55}}, \quad s_2 = \sqrt{I_1^2/(I_\circ I_2)}. \tag{17}$$

Clearly for non-trivial value of r, there should be axial-flexural coupling and the presence of asymmetric mass distribution across the beam thickness will give non-trivial s_2. If A_{55} becomes infinite, s_1 will be zero, which is the case of degeneracy from thick beam to thin beam. For non-trivial solution of the displacement field, Eq. (14) yields a sixth order characteristic polynomial in k_j, given by

$$ak_j^6 + bk_j^4 + ck_j^2 + d = 0, \tag{18}$$

where

$$a = 1 - r^2, \quad b = 2rs_1s_2k_ak_b^2/k_r - (1 - r^2)k_r^2 - s_1^2k_b^4/k_r^2 - k_a^2, \tag{19}$$

$$c = k_a^2k_r^2 - 2rs_1s_2k_ak_rk_b^2 - (1 - s_1^2)k_b^4 + s_1^2(1 - s_2^2)k_a^2k_b^4/k_r^2, \tag{20}$$

$$d = \left(1 - s_1^2(1 - s_2^2)\right)k_a^2k_b^2. \tag{21}$$

Since, Eq. (18) is a polynomial with even order terms, pairs of root have to exist, which are opposite in sign. Further, each of these pairs must be distinct and they represent axial, flexural and shear modes, respectively. The inference that can be drawn from above properties is that the axial mode must have strictly real wave numbers. The other modes may have complex wave numbers depending on the material configuration. Therefore, we first compute the real roots $\pm\sqrt{\alpha}$ corresponding to the forward and backward propagating axial modes ($j = 1, 2$), numerically. Next, the other modes ($j = 3, \ldots, 6$) are obtained explicitly. These can be written as

$$k_1, k_2 = \pm\sqrt{\alpha}, \tag{22}$$

$$k_3, k_4 = \pm\left[-\left(\frac{b + \alpha a}{2a}\right) + \left\{\left(\frac{b + \alpha a}{2a}\right)^2 - \frac{\alpha(b + \alpha a)}{a}\right\}^{1/2}\right]^{1/2}, \tag{23}$$

$$k_3, k_4 = \mp\left[-\left(\frac{b + \alpha a}{2a}\right) - \left\{\left(\frac{b + \alpha a}{2a}\right)^2 - \frac{\alpha(b + \alpha a)}{a}\right\}^{1/2}\right]^{1/2}. \tag{24}$$

Although there are more general methods for computation of general complex roots such as Müller's method (Müller, 1956) and Jenkins-Traub method (Jenkins and Traub, 1972), we shall stick to the above scheme. The reason is that the reordering of roots to track individual modes over a broad band of frequency (consisting of typically 8192 to 16384 sampling FFT points) will not be required in this procedure and it saves significant amount of computation time especially when different material properties are assigned to different elements.

3. Spectral element formulation

Here two different elements are formulated, one that is finite in length having two nodes and second is the one-noded throw-off element, whose second node is assumed to be at infinity. The element has 3 degrees of freedom per node as shown in Fig. 2(a).

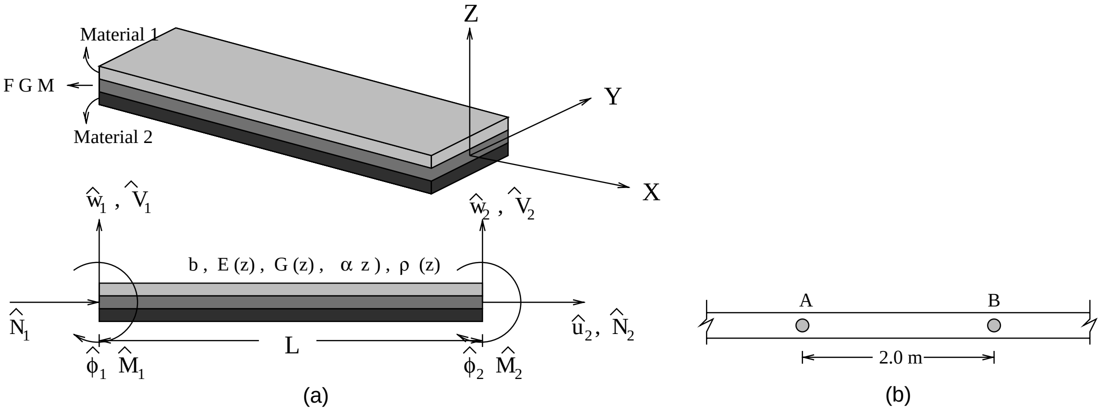

(a) (b)

Fig. 2. (a) Coordinate system and degrees of freedom for the spectral element and (b) beam geometry for modulated pulse load.

3.1. Finite length element

In what follows, the bold face capital letters denote matrices and the bold face small letters denote vectors. In the following derivation, first order shear deformable multi-material beam having three degrees of freedom per node (axial, transverse and rotational) is considered. Spectral element formulation begins with the solution of the governing equation in the frequency domain and determining the wave number associated with the motions. Using the solution of the governing equation as interpolation functions, an exact dynamic stiffness matrix is formed at each discrete frequency and the global assemblage is carried out in identical manner as in standard the FE method. The element nodal vectors of displacements, strains, stresses, forces etc. are dealt in terms of their respective spectral amplitudes. After computing the wave numbers at a particular frequency ω_n, the explicit form of the generic displacement vector can be rewritten from Eq. (13) as

$$\mathbf{u}(x,\omega_n) = \left\{ \begin{array}{c} \hat{u}(x,\omega_n) \\ \hat{w}(x,\omega_n) \\ \hat{\phi}(x,\omega_n) \end{array} \right\} = \begin{bmatrix} R_{11} & \cdots & R_{16} \\ R_{21} & \cdots & R_{26} \\ R_{31} & \cdots & R_{36} \end{bmatrix} \mathbf{D} \left\{ \begin{array}{c} \tilde{u}_1 \\ \vdots \\ \tilde{u}_6 \end{array} \right\}, \tag{25}$$

where $\mathbf{D}$ is a diagonal matrix with exponential entries, and can be expressed as

$$D_{jj} = \left\{ \begin{array}{ll} \mathrm{e}^{-\mathrm{i}k_j x}, & j = 1,3 \\ \mathrm{e}^{-\mathrm{i}k_j (L-x)}, & j = 4,6 \end{array} \right\}. \tag{26}$$

Here, L is the length of the element. Entries associated with $j = 1, 3, 5$ and $j = 2, 4, 6$ contribute to forward and backward propagating or evanescent components, respectively. This classification is to keep track of the individual wave modes as the computation proceeds from ω_n to ω_{n+1}. In Eq. (25), $\mathbf{R}$ denotes the amplitude ratio matrix, which can be derived by satisfying Eq. (13) and is expressed as

$$R_{1j} = 1, \quad \forall\, j \in [1,2], \quad R_{2j} = 1, \quad R_{3j} = \frac{\mathrm{i}(k_r^2 - k_j^2)}{k_j} \quad \forall\, j \in [3,6], \tag{27}$$

$$R_{1j} = \frac{\mathrm{i}\left(k_j^2 - k_r^2\right)\left(s_1 s_2 k_a^2/k_r - r k_a k_j^2/k_b^2\right)}{k_j\left(k_j^2 - k_a^2\right)} \quad \forall\, j \in [3,6], \tag{28}$$

$$R_{2j} = \frac{\mathrm{i}k_j\left(rk_r^2k_j^2/k_ak_b^2 - s_1s_2k_r\right)}{\left(k_j^2 - k_r^2\right)\left(1 - s_1^2 + k_r^2k_j^2/k_b^4\right)} \quad \forall\, j \in [1,2], \tag{29}$$

$$R_{3j} = \frac{\left(k_j^2 - k_r^2\right)\left(rk_r^2k_j^2/k_ak_b^2 - s_1s_2k_r\right)}{\left(k_j^2 - k_r^2\right)\left(1 - s_1^2 + k_r^2k_j^2/k_b^4\right)} \quad \forall\, j \in [1,2]. \tag{30}$$

Now, to form the element shape function matrix $\mathbf{N}(x,\omega_n)^e$, we consider Eq. (25) and eliminate the unknown wave coefficient vector $\tilde{\mathbf{u}}$ by using the nodal displacement vector $\hat{\mathbf{u}}^e$ as follows

$$\hat{\mathbf{u}}(x,\omega_n) = \mathbf{RD}\tilde{\mathbf{u}} = \mathbf{T_1}(x,\omega_n)\tilde{\mathbf{u}}, \tag{31}$$

$$\hat{\mathbf{u}}^e = \begin{bmatrix} \mathbf{T_1}(0,\omega_n) \\ \mathbf{T_1}(L,\omega_n) \end{bmatrix}\tilde{\mathbf{u}} = \mathbf{T_2}\tilde{\mathbf{u}}, \tag{32}$$

$$\hat{\mathbf{u}}(x,\omega_n) = \mathbf{T_1}(x,\omega_n)\mathbf{T_2}^{-1}\hat{\mathbf{u}}^e = \mathbf{N}(x,\omega_n)^e\hat{\mathbf{u}}^e. \tag{33}$$

In Eq. (32), the non-singular (6 × 6) complex matrix $\mathbf{T_2}$ represents the local wave characteristics of the displacement field. Next, the generic force vector is obtained from the force boundary conditions (Eqs. (9) and (10)) as

$$\hat{\mathbf{f}}(x,\omega_n) = \mathbf{Q_0}\hat{\mathbf{u}}(x,\omega_n) + \mathbf{Q_1}\frac{\partial}{\partial x}\hat{\mathbf{u}}(x,\omega_n) \tag{34}$$

and is evaluated at $x = 0$ and $x = L$ with the help of Eq. (31), which yields the element nodal force vector as

$$\hat{\mathbf{f}}^e = \begin{bmatrix} -(\mathbf{Q_0RD} + \mathbf{Q_1RD}')_{x=0} \\ (\mathbf{Q_0RD} + \mathbf{Q_1RD}')_{x=L} \end{bmatrix}\mathbf{T_2}^{-1}\hat{\mathbf{u}}^e = \widehat{\mathbf{K}}^e\hat{\mathbf{u}}^e, \tag{35}$$

where $\widehat{\mathbf{K}}^e$ is the (6 × 6) exact complex spectral finite element dynamic stiffness matrix. $\mathbf{Q_0}$ and $\mathbf{Q_1}$ are both (3 × 3) real matrices whose entries are the functions of stiffness coefficients A_{11}, A_{55}, B_{11} and D_{11}. $\mathbf{D}'$ is a (6 × 6) diagonal matrix obtained as

$$D'_{jj} = \frac{\partial}{\partial x}D_{jj}, \quad j = 1,\ldots,6. \tag{36}$$

3.2. Semi-infinite or throw-off element

The displacement field given by Eq. (25) has coefficients of both incident and reflected waves. The throw-off element is formulated by leaving out the reflected coefficients in the displacement formulation, which leads to an one-noded spectral element. This particular aspect is helpful when one needs to filter out any noise from near-field response for accurate estimation. In SEM, such analytic features of a single node semi-infinite spectral element is incorporated by modifying the amplitude ratio matrix as

$$\mathbf{R} = \begin{bmatrix} R_{11} & 0 & R_{13} & 0 & R_{15} & 0 \\ R_{21} & 0 & R_{23} & 0 & R_{25} & 0 \\ R_{31} & 0 & R_{33} & 0 & R_{35} & 0 \end{bmatrix}. \tag{37}$$

Use of this throw-off element in a structural boundary amounts relieving the trapped energy from the structure and hence as a result maximum damping can be artificially introduced in the structure.

3.3. Computational scheme

The SEM presented in this paper provides a key methodology to make wave propagation analysis suitable to incorporate within the framework of standard FE method. Since, the element dynamic stiffness matrix is derived by satisfying the coupled wave equations and forced boundary conditions exactly, one element is sufficient to model a uniform beam segment. This makes the global system which is many orders smaller compared to the time domain FE model for transient dynamic and wave propagation analysis. Any applied load history is represented as

$$\mathbf{f}(x,t) = \sum_{n}^{N} \hat{\mathbf{f}}(x,\omega_n)\,\mathrm{e}^{\mathrm{i}\omega_n t}. \tag{38}$$

Loading spectrum ($\hat{\mathbf{f}}$ for each ω_n in Eq. (38)) is obtained from the time dependent load history using forward FFT. The global system is first solved for unit impulse and hence the frequency response function (system transfer function) is determined directly. After solving, the actual spectral amplitudes of loading are convolved with the obtained frequency response. Similar to the time domain FE model, post-processing is then carried out before obtaining the time history by inverse FFT.

3.4. Treatment of distributed load

The original governing equations are non-homogeneous in nature and so far only the homogeneous part was considered for spectral element formulation. The non-homogeneous part occurs either in the form of distributed mechanical loading or temperature loading (which appears in the governing equations for spatially varying temperature). Hence, for complete solution of the problem, we need the particular solution of the governing equation (Eqs. (6)–(8)). There are two methods to get the particular solution. The first one is based on the direct solution to the particular integral and it involves symbolic computation. The second is the Ritz method based on stationarity principle in the frequency domain and this method is better suited for FE implementation. Only the second method is discussed here and implemented in SE code.

3.4.1. Variational principle in frequency domain

The product of spectral amplitudes of the conjugate quantities (stresses, strains and displacements) is represented as an energy equivalent measure in the frequency domain. Such a frequency domain energy functional in the context of virtual work principle is discussed in the work of Gopalakrishnan and Doyle (1994) and is not the same as the frequency domain counterpart (in terms of the convolution integral) of the time domain energy. Here, we define the frequency domain strain energy, kinetic energy and external work respectively as

$$\widehat{U}_S = \int_\Omega \hat{\sigma}^t \hat{\epsilon}\,\mathrm{d}\Omega, \quad \widehat{U}_I = -\int_\Omega \omega_n^2 \rho \hat{\mathbf{u}}^t \hat{\mathbf{u}}\,\mathrm{d}\Omega, \quad \widehat{V} = -\int_\Gamma \hat{\mathbf{p}}^t \hat{\mathbf{u}}\,\mathrm{d}\Gamma - \hat{\mathbf{f}}^t \hat{\mathbf{u}}, \tag{39}$$

where $\hat{\sigma}$, $\hat{\epsilon}$, $\hat{\mathbf{u}}$ and $\hat{\mathbf{p}}$ are the stress, strain, displacement and the distributed loading in frequency domain. Ω and Γ are the domain and boundary of the system. At each sampling frequency ω_n, the continuous system reduces to a stationary system in Eq. (39). The principle of virtual work in the frequency domain states that

$$\delta(\widehat{U}_S + \widehat{U}_I + \widehat{V}) = 0. \tag{40}$$

Following the same procedure as in the standard FE formulation, the shape function to interpolate the field variables are assumed and taken in the form given in Eq. (33), which yields the equilibrium equation in terms of nodal variables in the frequency domain as

$$\widehat{\mathbf{K}}\hat{\mathbf{u}} = \hat{\mathbf{f}} + \int_{\Gamma} \mathbf{N}^t \hat{\mathbf{p}}\,\mathrm{d}\Gamma, \quad \text{where } \widehat{\mathbf{K}} = \int_{\Omega} \mathbf{B}^t \overline{\mathbf{Q}} \mathbf{B}\,\mathrm{d}\Omega - \int_{\Omega} \omega_n^2 \rho \mathbf{N}^t \mathbf{N}\,\mathrm{d}\Omega. \tag{41}$$

Upon choosing $\hat{u}(x, \omega_n)$ as the Ritz function the essential boundary conditions are automatically satisfied. In addition, since $\hat{u}(x, \omega_n)$ is derived by satisfying the governing homogeneous wave equations exactly, it can be shown that dynamic stiffness matrix obtained in Eq. (41) is identical to the spectral element stiffness matrix obtained in Eq. (35). Here, **B** is the complex spectral element strain displacement matrix. The integral term in left equation of Eq. (41) represents the consistent nodal force vector due to distributed load $\hat{\mathbf{p}}$.

3.4.2. Load vector due to temperature

For the spectral analysis, the temperature $\Delta T(x, t)$ is transformed into frequency domain through a Fourier transformation given by

$$\Delta T(x, t) = \sum_{1}^{N} \Delta \widehat{T}(x, \omega_n)\,\mathrm{e}^{-\mathrm{i}\omega_n t}, \tag{42}$$

where the $\Delta \widehat{T}(x)$ is spatially varying. The consistent nodal force vector can be obtained from Eq. (41), by replacing $\hat{\mathbf{p}}$ with $\Delta \widehat{T}(x, \omega_n)$. Hence, the consistent load vector arising from variational formulation is given by

$$\hat{\mathbf{f}}_1^e = \int_0^L \mathbf{N}(\mathbf{x}, \omega_n)^t \begin{Bmatrix} -AT_{11}\Delta\widehat{T}_{,x} \\ 0 \\ BT_{11}\Delta\widehat{T}_{,x} \end{Bmatrix} \mathrm{d}x. \tag{43}$$

For all the cases of temperature variation, (constant or spatially varying temperature rise), from boundary conditions (Eqs. (9) and (10)), the element load vector is obtained as

$$\hat{\mathbf{f}}_2^e = \left\{ AT_{11}\Delta\widehat{T}(0) \;\; 0 \;\; -BT_{11}\Delta\widehat{T}(0) \;\; -AT_{11}\Delta\widehat{T}(L) \;\; 0 \;\; BT_{11}\Delta\widehat{T}(L) \right\}^t. \tag{44}$$

In all numerical cases considered here for temperature load, only spatially constant temperature rise is analysed and for this simplified case, the element load vector becomes

$$\hat{\mathbf{f}}_\circ^e = \Delta\widehat{T}_\circ \{ AT_{11} \;\; 0 \;\; -BT_{11} \;\; -AT_{11} \;\; 0 \;\; BT_{11} \}^t, \tag{45}$$

where $\Delta\widehat{T}_\circ(\omega_n)$ is the spatially rise in temperature.

4. Results and discussions

In all the numerical experiments performed in this work, a beam of unit width and 0.05 m depth is taken. Unless specified otherwise, a three layer beam is considered in the study. The top layer is that of steel of thickness 0.01 m and the bottom layer is alumina of 0.031 m. In between, there is an FGM layer of 0.009 m thickness, which blends all the mechanical and thermal properties of alumina and steel smoothly according to the power law (Eq. (5)) with exponent $n = 1.5$. Properties of steel are assumed as $E = 210$ GPa, $G = 80$ GPa, $\rho = 7800$ kg/m^3, $\alpha = 14.0 \times 10^{-6}$ °C^{-1} and that of alumina are $E = 390$ GPa, $G = 137$ GPa, $\rho = 3950$ kg/m^3, $\alpha = 6.9 \times 10^{-6}$ °C^{-1}, where E, G, ρ and α are Young's modulus, Shear modulus, density and coefficient of thermal expansion, respectively.

The spectrum and dispersion relation for these material properties are computed by the methods discussed earlier and plotted. In Fig. 3, dispersion of wave numbers corresponding to axial, flexure and shear modes are shown. From this figure, we can say that the axial speed is higher than the bending speed but lower than the shear speed because it has a slope that is in between two and the group speed (C_g) is the

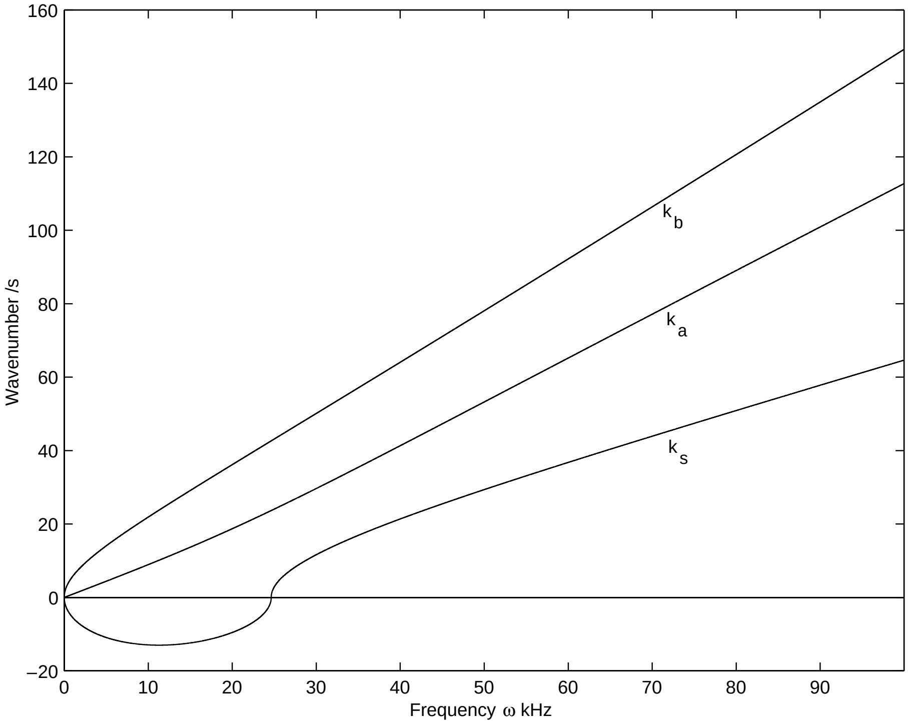

Fig. 3. Spectrum relation: (subscript *a*, *b* and *s* denote axial, bending and shear respectively).

inverse of this slope ($C_g = Re\{d\omega_n/dk_j\}$). To see how the wave packets travel at different frequencies, group speeds in axial, flexural and shear modes are plotted in Fig. 4. From these two plots it can be observed that there exists a cut-off frequency for shear mode

$$\omega_{\text{cut-off}} = \sqrt{\frac{A_{55}}{I_2(1 - s_2^2)}} \tag{46}$$

above which the shear mode starts propagating which is otherwise an evanescent component contributing to the flexural wave. Eq. (46) is obtained by putting $k_j = 0$ in Eq. (18) and solving for ω_n. In general, it can be said that at higher frequencies, all the group speeds become more or less constant.

Cut-off frequency is one parameter that determines the need for higher order beam theory. In elementary beams, the cut-off frequency is at infinity i.e. shear mode appears as evanescent mode which never propagates. If the frequency of interest is within the occurrence of the cut-off frequency, then the elementary beam theory is sufficient to predict the response. In this study, we have used FSDT, where the shear mode, which is evanescent to start with, begins to propagate beyond cut-off frequency. The cut-off frequency given by Eq. (46) is a function of the exponent n (Eq. (5)) and the thickness of FGM layer (h_{fgm}). Hence, it would be interesting to see the shifting of cut-off frequency with the change in the value of n and the thickness of FGM layer. Fig. 5 shows the variation of cut-off frequency with $\beta = h_{\text{fgm}}/h$, for different values of n. Here, h is the total depth of the beam. From Fig. 5, it can be seen that, for $n = 1$, there is a small decrease in the cut-off frequency with increase in value of β. When $n = 1.2$, the cut-off frequency does not show any dependence over β. For all values of n greater than 1.2, cut-off frequency increases with increase in the value of β. Hence, it can be concluded that the introduction of FGM layer shifts the cut-off frequency to a higher value

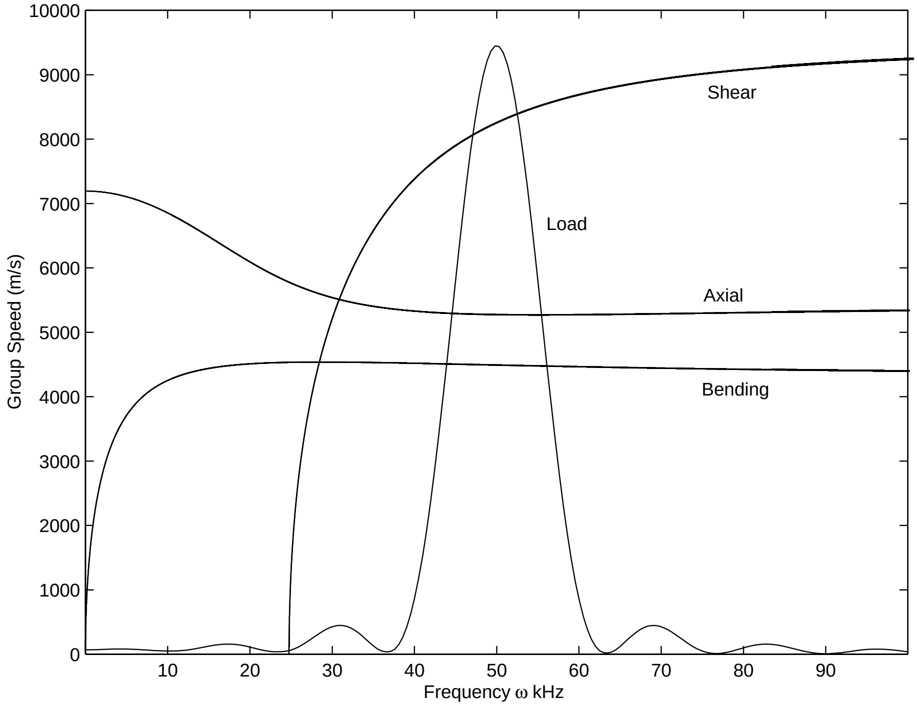

Fig. 4. Dispersion relation.

and from the Fig. 5, it can be seen that this shift is maximum (15%) when the beam is a full FGM beam ($\beta = 1$).

Next, three different problems are designed to bring out the essential features of wave propagation in FGM beam. In the first example, the axial and flexural wave propagation due to an impact load in a cantilever beam is studied. The aim of this example is to not only validate the element with conventional FE solution, but also study the dynamic stress smoothening effect in FGM beam due to material mismatch at the interface. In the next example, the behavior of FGM beam to transient temperature loading is studied. Here, two different temperature load history is considered, one having very high frequency content and the other having moderate frequency content. The final example considered here will demonstrate the presence of axial-bending-shear coupling in the FGM beam.

4.1. Impact on a cantilever FGM beam: verification with conventional FE solution

First, the validity of the analysis using the formulated element is established by comparing the obtained wave propagation results with both 2D and 1D FE solutions (Chakraborty et al., 2002). For this purpose, a cantilever beam of 1.0 m length with material and cross-section as specified earlier is taken and a load as shown in Fig. 6 is applied at the free end, first axially and then transversely. To model the FGM beam for 2D FE analysis, a mesh of 10,000 plane stress constant strain triangular elements is used where the depthwise property variation is modeled with five layers of elements and each layer having constant material properties. The top and the bottom layers are allocated to steel and alumina while the middle three layers are modeled as FGM material, with material properties distributed according to power law ($n = 1.5$)

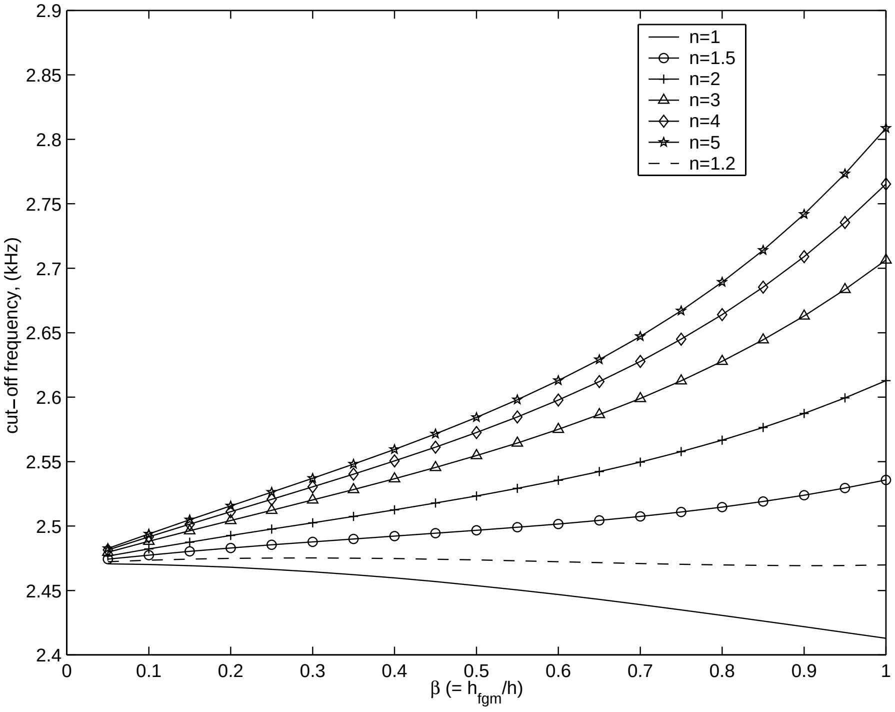

Fig. 5. Variation of cut-off frequency with β for different values of n.

and SBS method ($V_{p1} = 0.001$), as stated before. This approach is taken for modeling the FGM layers in the absence of a genuine 2D FGM finite element. Hence, it is expected that such a model will introduce approximations (both in amplitude and period) in the overall wave responses, due to approximate nature of mass distribution. These approximations can be overcome by taking a very fine mesh in the FGM layer. In the present study, total system size for 2D analysis is $19,988 \times 15$ (where 15 is half-bandwidth). For 1D FE analysis, 1000 elements are considered which gives a system size of 2997×6 where 6 is half-bandwidth. Compared to such large system sizes, only one spectral element is sufficient in SEA and the system size is only 3×3. This significantly reduces the computational effort by many orders, which is quite unlikely for both 1D and 2D FEA. In SEM, the number of FFT points considered are 16,384 at a sampling rate of 1 μs.

The cantilever beam is impacted at the tip with the load whose time and frequency domain representation is shown in Fig. 6. The figure shows that the pulse is of 50 μs duration, having a frequency content of around 46 kHz. The response of the beam to such a high frequency short duration loading brings several basic features of wave phenomena. As seen in Fig. 7, where the axial velocity due to the axial load is plotted with time, the incident axial wave is initially non-dispersive and after it gets reflected from the fixed boundary, it starts to become dispersive. This is one of the fundamental feature of the coupled wave propagation problem. The incident response from SEA matches well with both 2D and 1D FEM analysis, however there is mismatch of magnitude of reflected pulse with the 2D FEM results. This can be attributed to the approximate material property variation considered in the 2D model. There is little difference among the SEA responses predicted by the power law and SBS method at the reflection from boundary.

Fig. 8 gives the transverse velocity history of the FGM cantilever beam due to transverse load. Unlike the axial wave, the response is dispersive throughout. As in the previous case, 1D formulation matches well with SEA solution. However, 2D FE solution only predicts the incident flexural wave accurately. Ap-

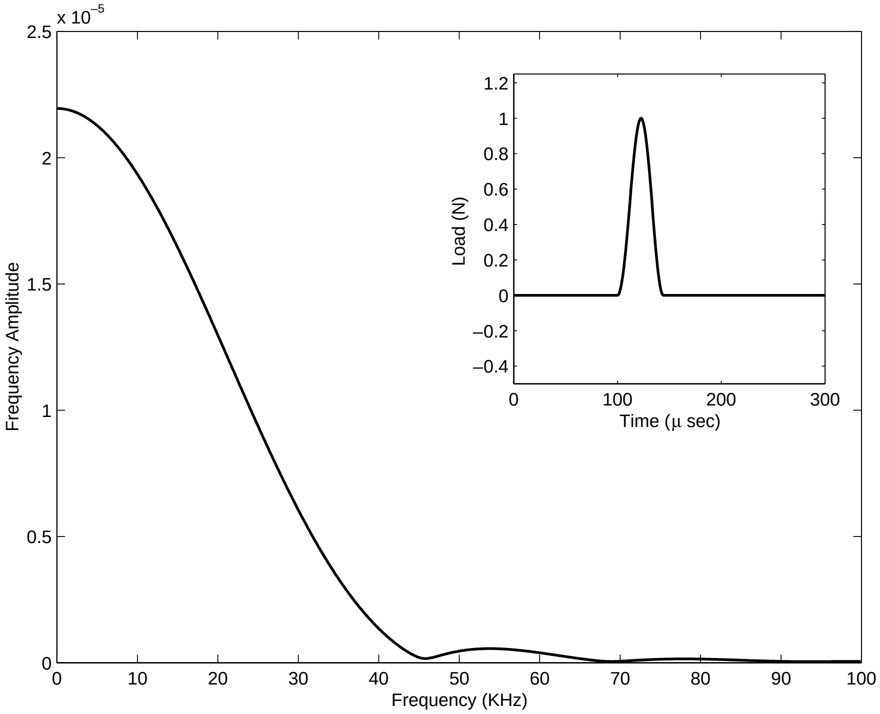

Fig. 6. Triangular pulse with time representation inset.

proximate property distribution in the 2D FE modeling is causing the flexural wave to travel faster and as a result, the reflection arrives earlier than the 1D FE or Spectral Element solution and phase error occurs.

4.2. Stress smoothing effect in a FGM beam

As demonstrated in the previous section, the formulated spectral element has excellent capability to analyse wave propagation behavior in FG beam. One of the fundamental reason of using FGM in structures is to smoothen the stress jumps that normally occurs at the bi-material interface. This example will demonstrate as to how the stress smoothening can be accomplished using either a full FGM layer across the depth or a small FGM layer in the middle of the two parent material.

Same cantilever beam used in the previous study, is again considered here and the same pulse load (Fig. 6) is applied again at the tip axially. Stresses are measured at the middle of FGM layer ($z = 0.0$ m) and the alumina layer ($z = -0.02$ m) at the tip of the beam. Fig. 9 shows the variation of axial stress due to the axial load. The figure shows that the stress in FGM layer is almost four times larger initially and gradually this stress is alleviated through a smooth transfer to the alumina layer as seen in the first reflection (at 350 μs). Shear stress remains same for all the materials for all the times as can be seen in Fig. 10. Fig. 11 shows the axial stress history due to transverse load. From the figure, it is clear that the FGM layer experiences stresses which is mostly of opposite sign to that of the alumina layer. Even here, the FGM bears larger stress than alumina layer. The shear stress history due to transverse load is plotted in Fig. 12, where, as before, there is very little difference in magnitude between the stresses in the FGM and the alumina layer.

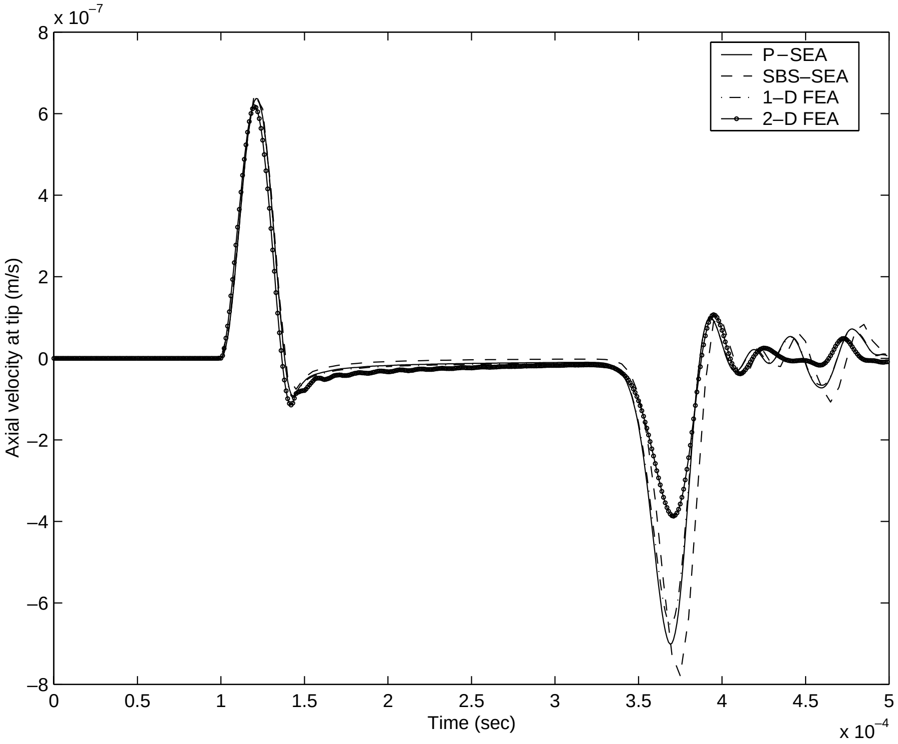

Fig. 7. Axial velocity at tip due to axial load.

Hence, it can be inferred that a small FGM layer can indeed reduce the large stress jump by gradually and smoothly transversing the stresses at the bi-material interface.

Next the depthwise stress variation is studied more closely. The same cantilever beam, subjected to axial impact is again considered here and the axial stress history at five different points are plotted in Fig. 13. The points are taken at $z = 0.0145$, 0.0045, −0.0045, −0.02 and −0.0355, where $z = 0$ denotes middle of FGM layer. From the geometry of the cross-section and thickness of each layer, the points considered correspond to the topmost layer, the interface of FGM and steel, interface of FGM and alumina, middle of alumina layer and the bottommost layer respectively. From the plot, it can be seen that the incident stress is maximum in the extreme fibres and at the bottom fibre, they are compressive in nature as expected. The reflected stress wave in all the cases are compressive and the smooth transfer of stress from steel to alumina causes maximum reflected response in the bottom alumina layer. To observe the smooth variation of stresses in FGM beam, the same cantilever beam with full FGM material is taken and impacted axially at the tip as before. The axial stress history at five different points (distributed equally along the depth, where $z = 0.025$ and $z = -0.025$ correspond to top and bottom layer respectively) are plotted in Fig. 14. Comparing with Fig. 13, it can be seen that, for full FGM beam, incident axial stress variation between layers are less compared to Fe–FGM–alumina beam and they are symmetric about the middle plane ($z = 0$) and no part of it is in compression until the reflection from the boundary arrives. The plot also shows that the magnitude of the reflected pulse decreases across the depth with the increase in distance from the middle plane. Variation of the axial stress with depth at times corresponding to the occurrences of incident and reflected waves is plotted in Figs. 15

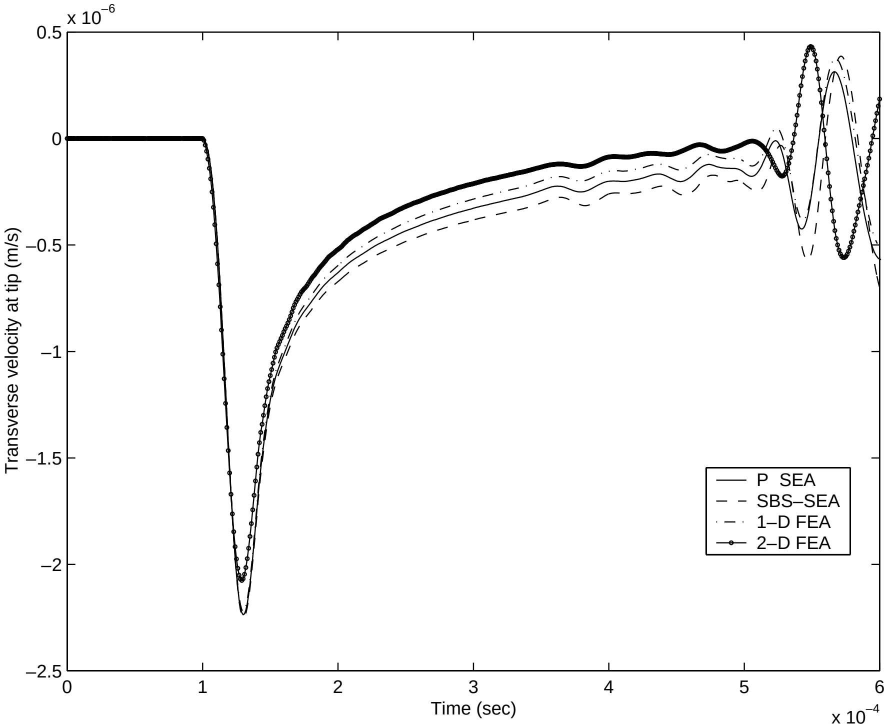

Fig. 8. Transverse velocity at tip due to transverse load.

and 16, respectively. The filled circles in these figures denotes FGM–steel and FGM–alumina interface. The stresses are sampled typically at those points where stress reaches its maximum values i.e. between 75 and 170 μs and 340 and 390 μs (which correspond to incident wave and reflection coming from the fixed end). The smoothening activities of FGM can be clearly seen from these two figures. In the absence of FGM material in between, the stress pattern will be that obtained by extending the stress lines above and below $z = 0$ in the direction of arrows upto the point $z = 0$ with same gradient, as shown in the figure. From Fig. 15, at time $t = 130$ μs, it can be seen that the FGM smoothens the axial stress of about 8 N/m^2, which is around 25% of the maximum stress involved and at 110 μs, FGM smoothens around 15 N/m^2, which is 50% of the maximum stress. Similarly, when the reflection arrives at the tip, Fig. 16 suggests that the absence of FGM will cause a stress jump of around 17 N/m^2 at time $t = 360$ μs. Fig. 17 shows the depthwise variation of stress for full FGM beam, for all times. The figure clearly shows the smooth transition of the axial stress across the depth. Thus, this example ascertains that the FGM effectively alleviates stress jump in dynamic loading cases.

4.2.1. Variation of the maximum stress gradient with FGM content and material law

The previous example has shown the stress smoothening property of the FGM across the depth. From Eq. (3), it is clear that the stress variation is a function of both the power exponent n (in Eq. (5)) as well as the depth of the FGM layer h. Here, the effect of the stress gradient $\mathscr{S} = \partial\sigma/\partial z$ is plotted against $\beta = h_{\mathrm{fgm}}/h$, which is shown in Fig. 18. From the figure, it is seen that for all values of n, the stress gradient $\mathscr{S}$ is high for small thickness of FGM layer (infinity for $h_{\mathrm{fgm}} = 0$), which is expected. This gradient reduces for increase in the value of n and the thickening of FGM layer. Fig. 19 shows the variation of $\partial\mathscr{S}/\partial n$ for

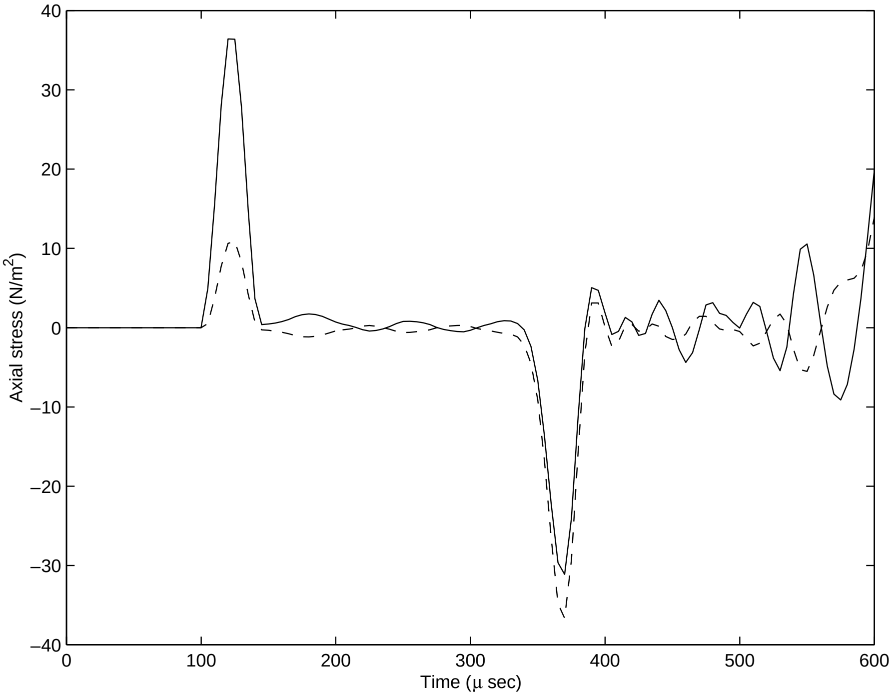

Fig. 9. Axial stress at tip due to axial load: (—) FGM layer and (- - -) alumina layer.

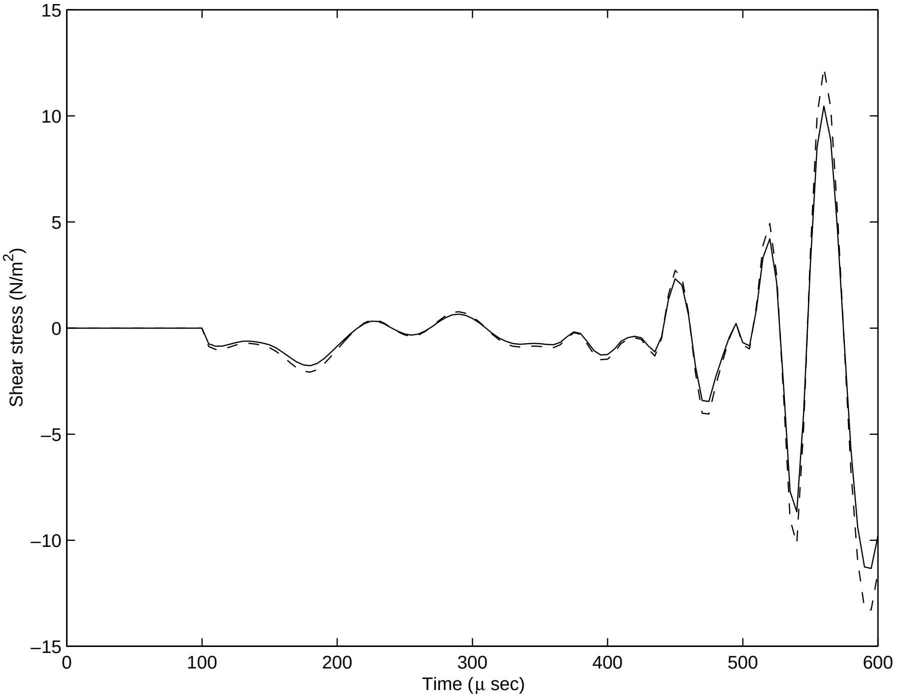

Fig. 10. Shear stress at tip due to axial load: (—) FGM layer and (- - -) alumina layer.

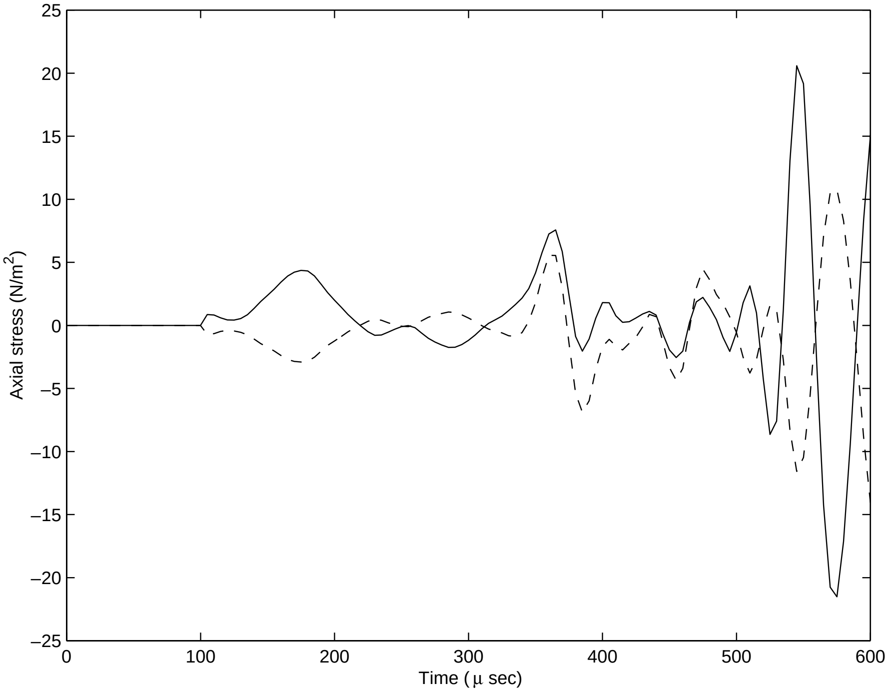

Fig. 11. Axial stress at tip due to transverse load: (—) FGM layer and (- - -) alumina layer.

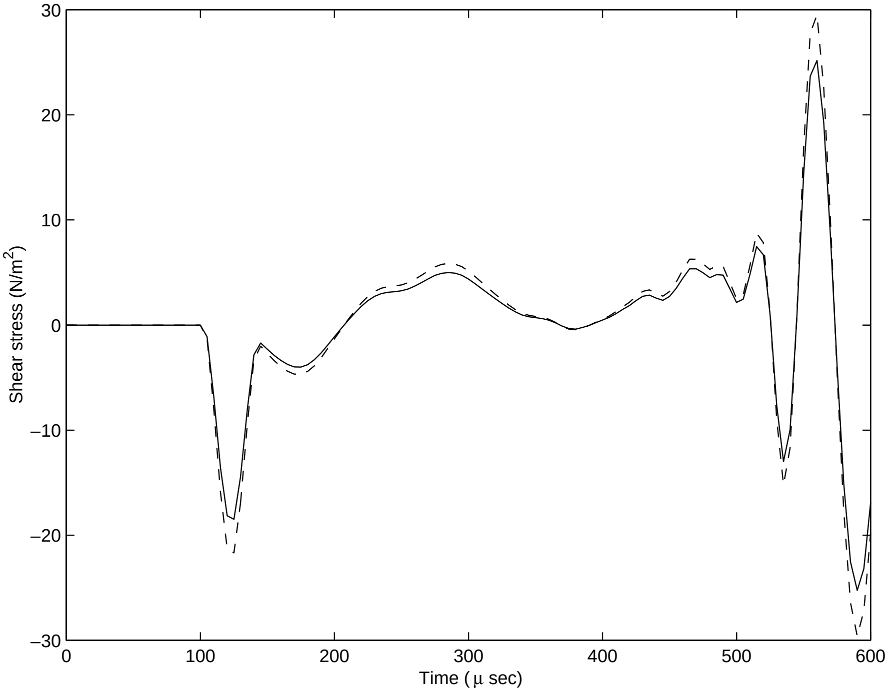

Fig. 12. Shear stress at tip due to transverse load: (—) FGM layer and (- - -) alumina layer.

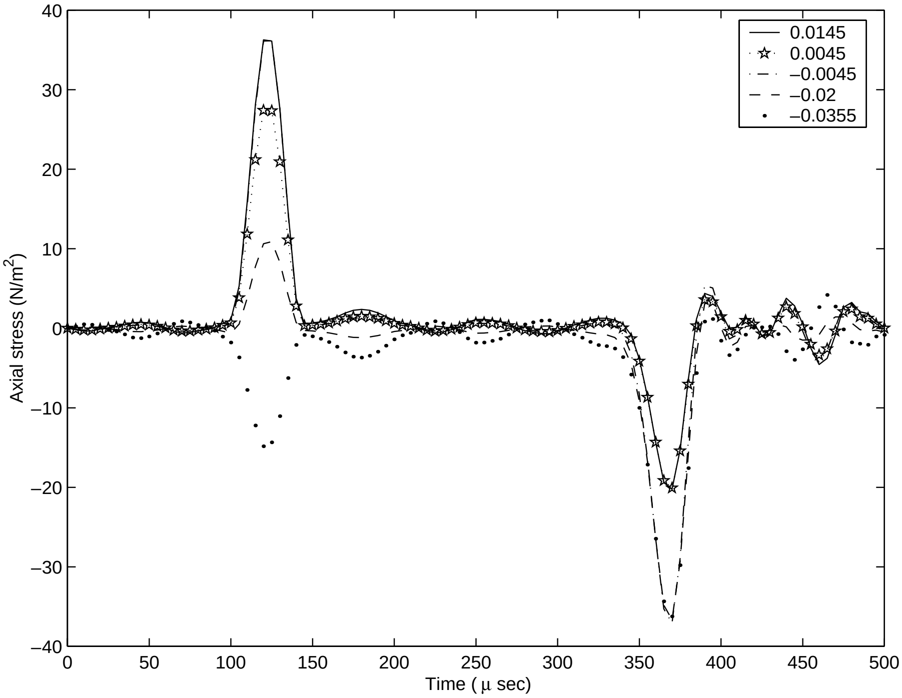

Fig. 13. Axial stress at tip due to axial load (Fe–FGM–alumina beam): legend indicates *z* (depth) coordinate.

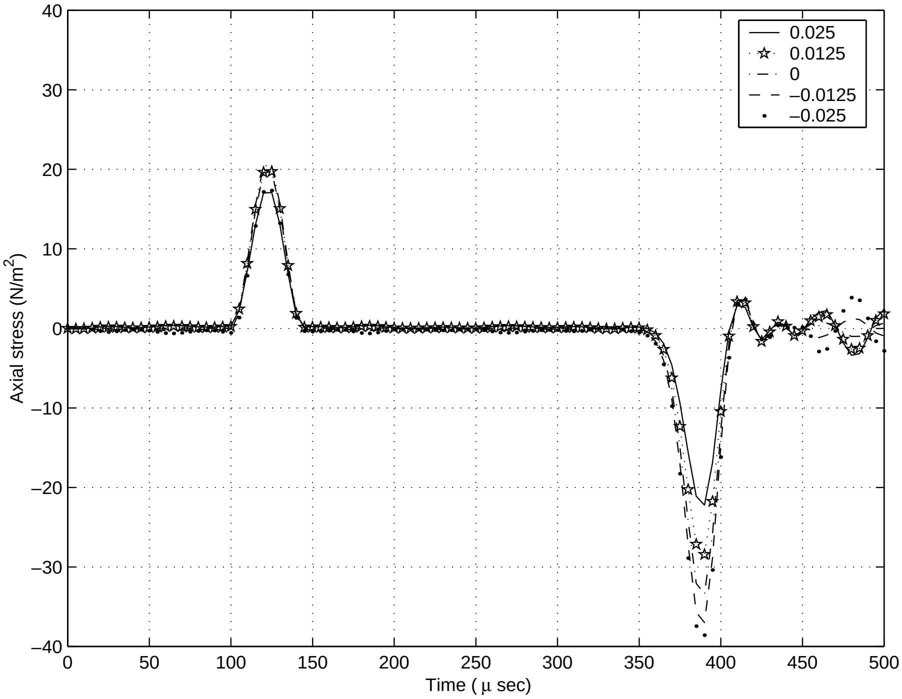

Fig. 14. Axial stress at tip due to axial load (full FGM beam): legend indicates *z* (depth) coordinate.

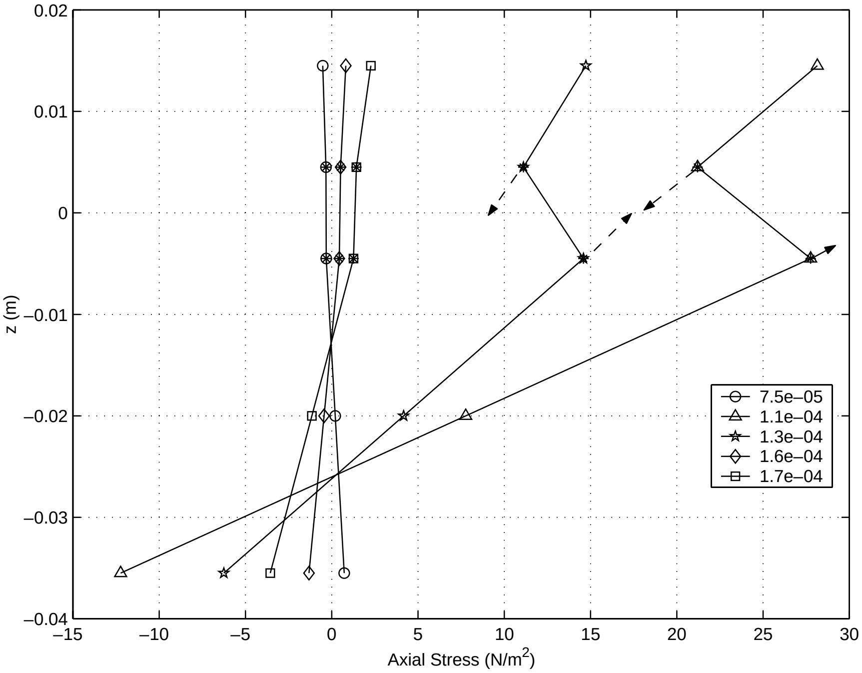

Fig. 15. Axial stress pattern at tip due to axial load at incident wave: legend indicates time of measurement.

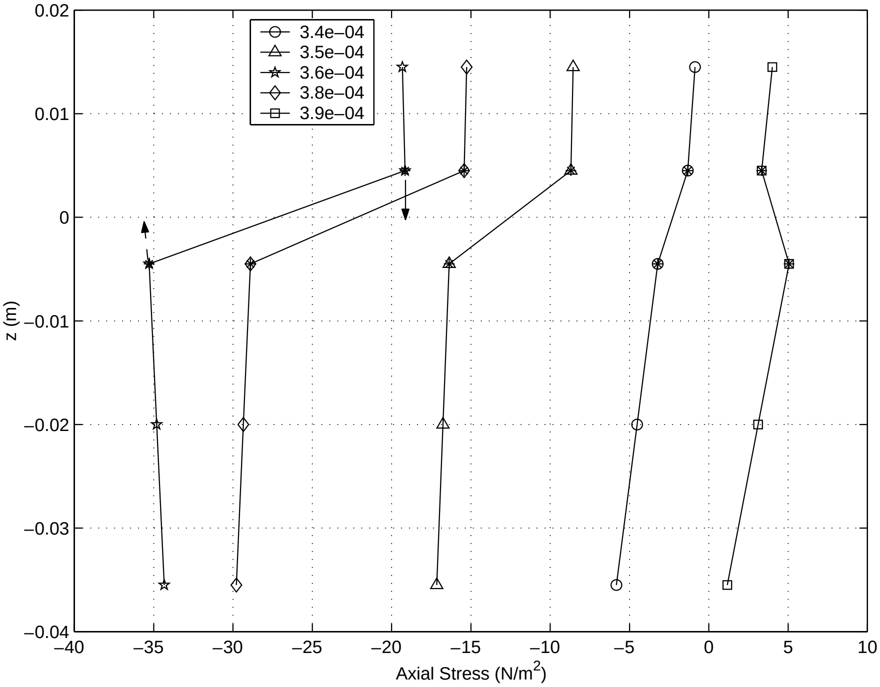

Fig. 16. Axial stress pattern at tip due to axial load at reflected wave: legend indicates time of measurement.

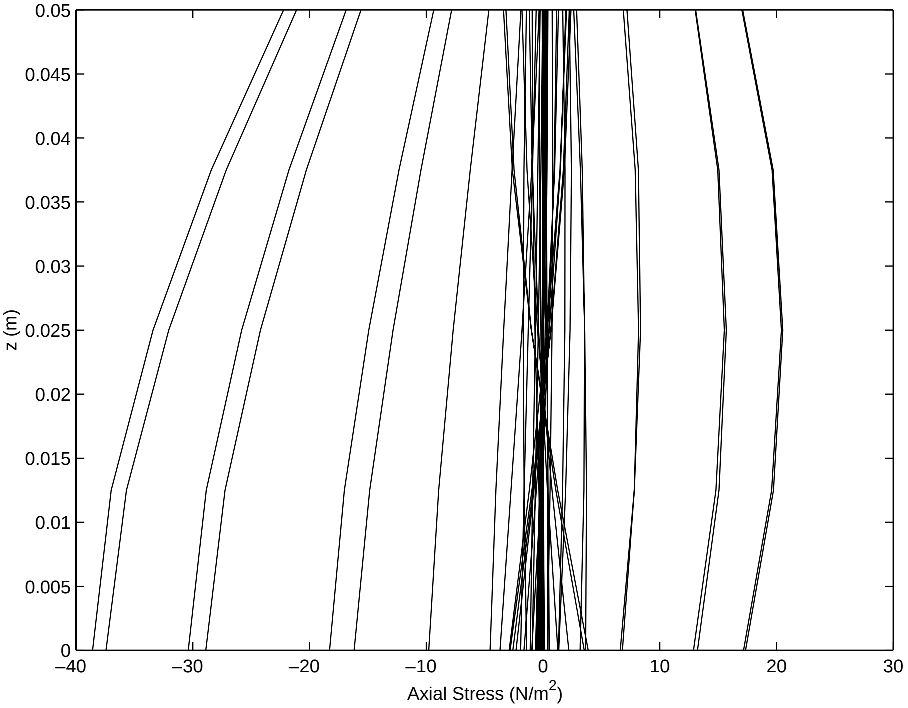

Fig. 17. Axial stress pattern at tip due to axial load for full FGM beam.

different values of n and FGM layer thickness. The figure shows negligible change in the values of $\partial\mathscr{S}/\partial n$ with increase in n and β. Hence, it can be concluded that the stress gradient is invariant to the exponent n.

4.3. Wave propagation due to highly transient temperature burst

Present spectral element can effectively handle thermal loading without taking temperature as nodal degrees of freedom. Since, it is the wave propagation phenomena that is of present interest in this paper, temperature loading is also taken as a short duration pulse having very high to moderate frequency content. For simplicity, it is assumed that $\Delta\widehat{T}(x,\omega_n)$ is spatially constant and this means that the load vector is as given by Eq. (45) for constant temperature rise $\Delta T_\circ$. Two different kind of temperature histories are considered here, one having moderate frequency content and the second one having high frequency content. The first one is ramp loading as shown in Fig. 20 and the second one is pulse loading as shown in Fig. 6.

The same cantilever beam with geometry and material property as taken earlier is considered here. The temperature of the beam is raised by 1 milli centigrade ($\Delta\widehat{T}^\circ$) and the velocity response of the beam is observed. Since, loading due to temperature is mainly axial in nature (in the present problem $AT_{11}/BT_{11} \approx 1000$), for the two load cases only axial responses are measured.

The ramp loading, as shown in Fig. 20, has moderate frequency content of 10 kHz as compared to the pulse loading. Such a load occurs in the real world situations, wherein the materials Steel and alumina are thermally fused with such a temperature profile. The load is applied to the beam with a constant temperature rise (1 milli degree centigrade) throughout the beam. The axial response of the beam at tip is plotted in Fig. 21. It can be observed that the initial response are small and response starts to pick up after

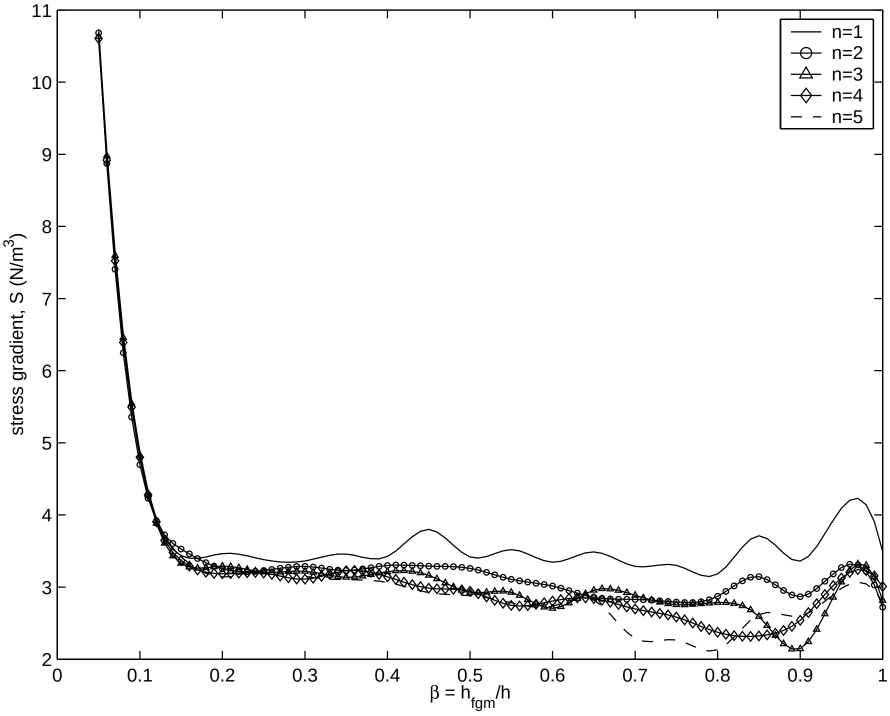

Fig. 18. Variation of maximum stress gradient ($\mathscr{S}$) with β for different values of n.

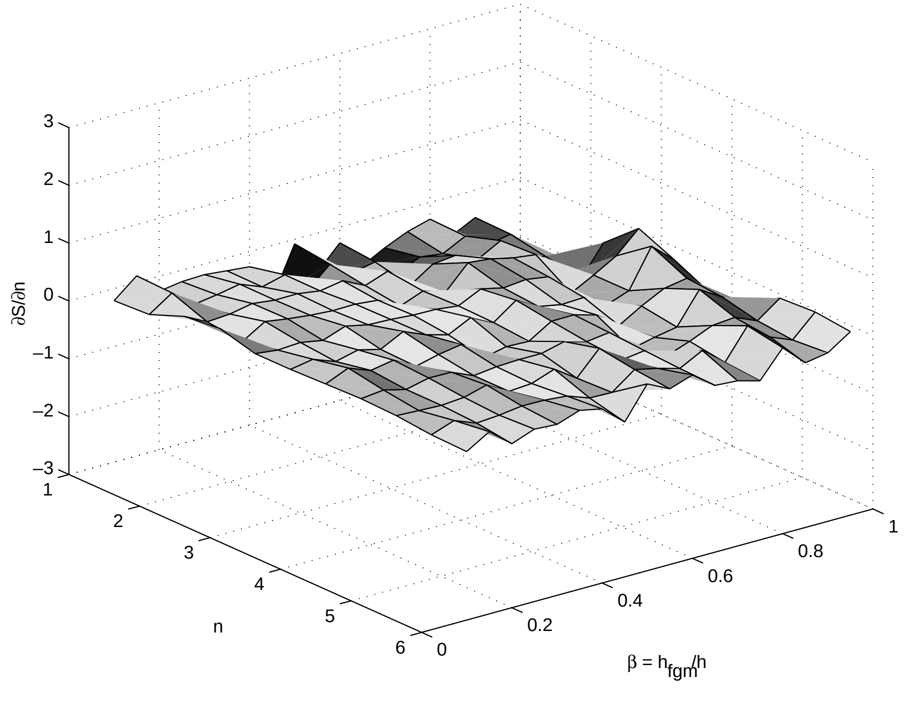

Fig. 19. Variation of $\partial\mathscr{S}/\partial n$ with n and β.

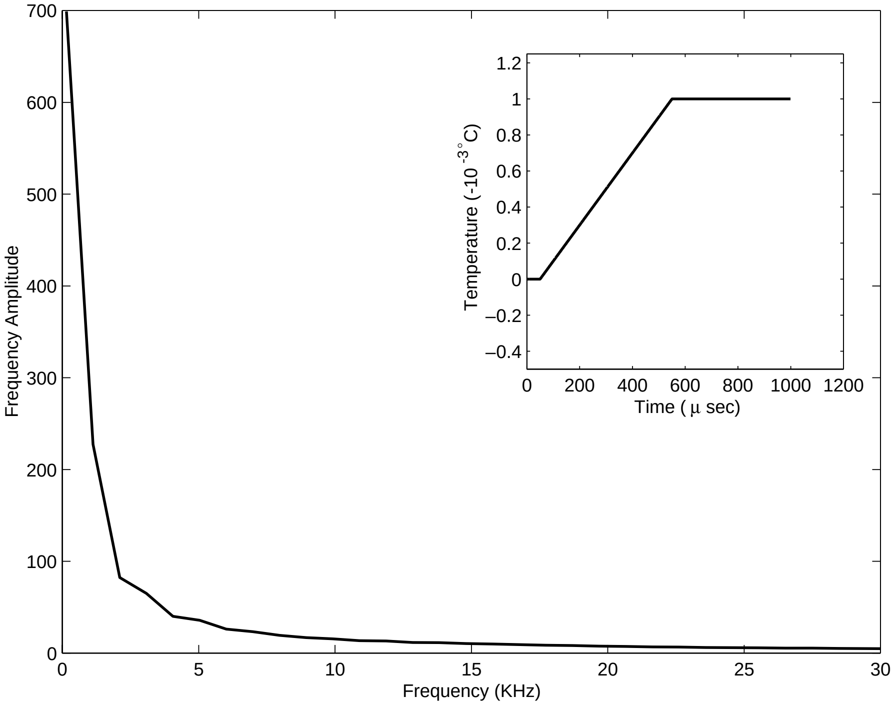

Fig. 20. Ramp loading with time domain data inset.

the temperature reaches the constant value of 1 milli °C. The end of the load marks a release in temperature and this set forths an impulse loading whose instantaneous response is observed at 1000 μs and the waveform continue to propagate.

Next, the pulse load is applied and the response of the beam is plotted in Fig. 22. Like in the mechanical loading case, the waves are initially non-dispersive and tend to become dispersive after first reflection occurs. The wavy nature and shootoff at selected points can be attributed to the small transverse load component that is present due to bending axial coupling. The response is compared with 1D FEA solution and as seen, they agree quite well.

4.4. Response to modulated pulse

One of the fundamental difference in wave behavior between the all Steel or alumina beam with the FGM beam is the presence of the axial-bending coupling. If the beam is thick, then an additional propagating shear wave is created, hence giving a three way axial-bending-shear coupling. The aim of this example is to demonstrate this effect in the FGM beam. In general, for an isotropic beam, the axial loading do not induce a bending mode (and vice-versa), as there is no axial-flexural coupling. In the present case, presence of FGM layer introduces an axial-flexural coupling and this is reflected in the non-zero r and s_2 (Eq. (17)). The impulse kind of loading (Fig. 6), which was applied earlier contains a band of frequency highly unsuitable for mediums which are highly dispersive, to capture all the different modes. The wave in FGM beam is also highly dispersive and hence such a impulsive load is not suitable for capturing propagating modes. Hence, if the contributions of each modes (axial, flexural and shear) are to be distinguished clearly, a pulse modulated at a certain constant (high) frequency beyond the cut-off frequency (Eq. (46))

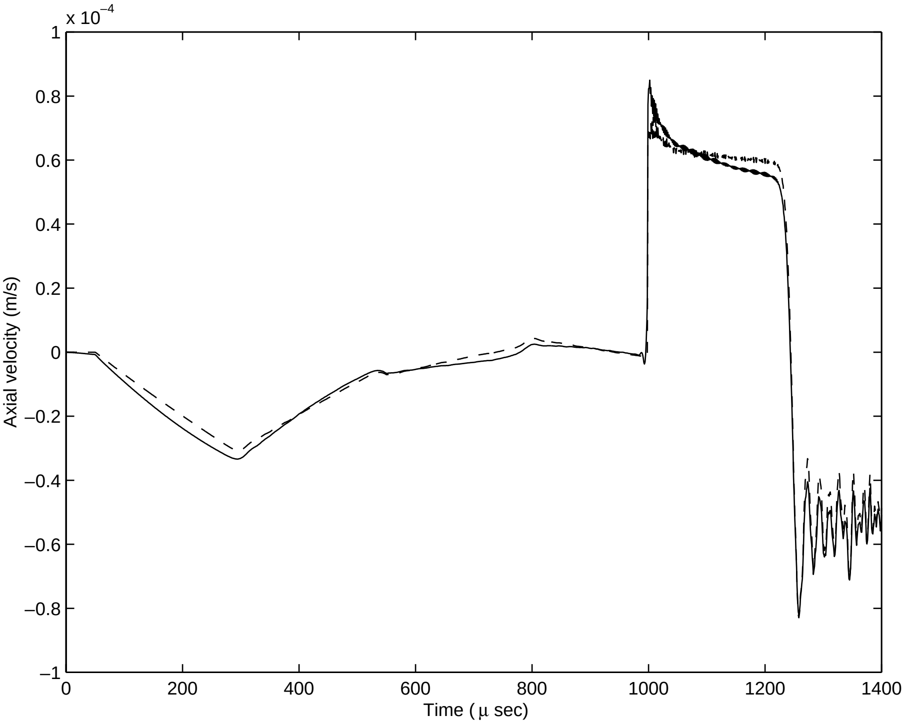

Fig. 21. Axial velocity at tip due to ramp kind temperature rise: (—) SEM and (- - -) 1D FEM.

needs to be applied. To capture different propagating modes, an infinite beam is taken where the cross-sectional and material properties are same as that for cantilever beam. It is assumed that the material properties vary according to power law with exponent $n = 1.5$. The spectrum relation and dispersion relation for this beam geometry and material properties are given in Figs. 3 and 4 respectively. The dispersion relation shows that the beam has cut-off frequency of 24.65 kHz. Hence, to observe propagating shear mode the loading pulse should be modulated above this frequency. Here, a pulse modulated at 50 kHz is taken and applied at a point A (see Fig. 2(b)) in the infinite beam, first axially and then transversally. At a distance of 2 m from the impact site (point B), the axial and transverse velocity response is measured for both the loading. Infinite portion of the beam is realized by using throw-off element on both side of a finite length element. Hence, the total number of elements used in this case is three (two throw-off and one finite length). The velocity response obtained is plotted in Fig. 23. From the dispersion relation (Fig. 4), group speeds of different propagating modes can be found and using these the occurrences of different modes can be computed. In Fig. 23, star mark in time axis denotes time of appearance of modes predicted by the dispersion relation. It is evident from the dispersion relation that, first mode will be shear, the next axial and last comes the bending wave. Axial and transverse velocity history due to axial load is shown in Fig. 23(a) and (b). As seen there, shear mode propagates along with bending and axial modes, although contribution of bending mode in axial velocity is much small compared to its contribution in transverse velocity. The axial and transverse velocity response due to transverse load is shown in Fig. 23(c) and (d). It can be observed that for the axial response, magnitude of all the modes are comparable, however, for the transverse velocity response, the axial and shear contribution is very less compared to the bending contribution. For all these cases, dispersion relation predicts the arrival of each mode quite accurately.

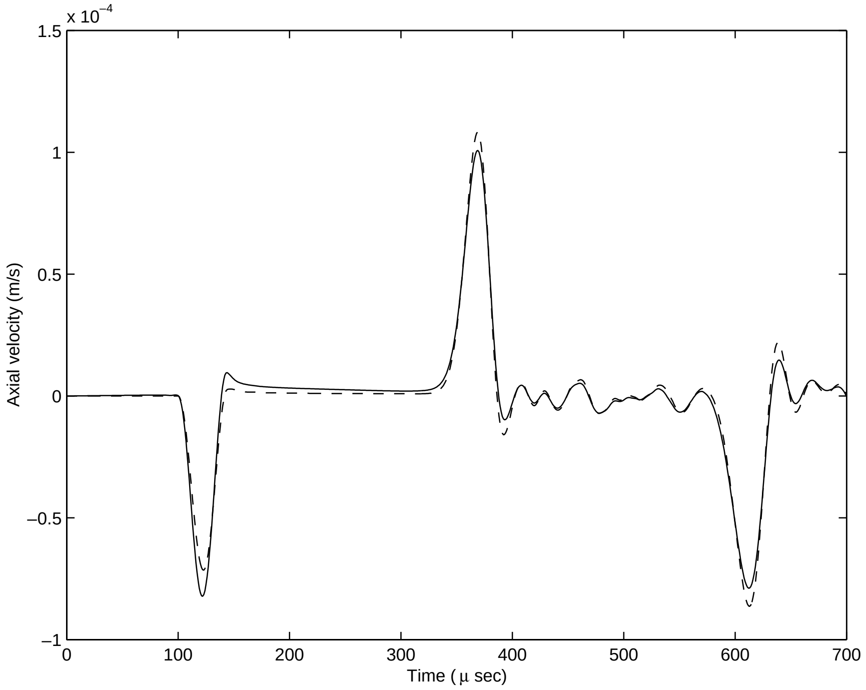

Fig. 22. Axial velocity at tip due to pulse kind temperature rise: (—) SEM and (- - -) 1D FEM.

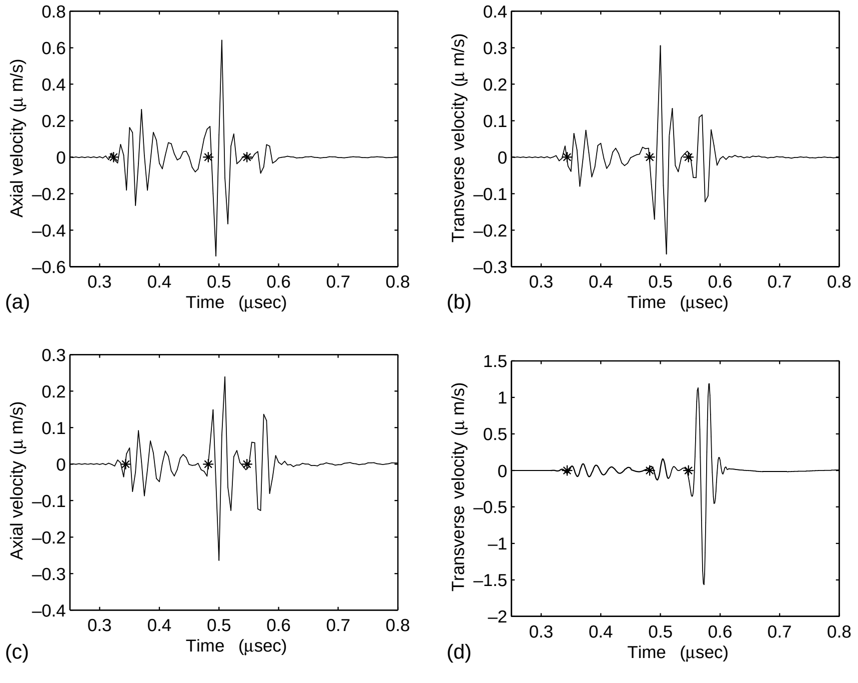

Fig. 23. Response to modulated pulse.

5. Conclusion

A novel spectral element is presented to study the wave propagation behavior in FGM beams subjected to high frequency impact loads. The element, based on first order shear deformation theory has exact dynamic stiffness matrix and it takes into account depthwise variation of material properties. Structures, subjected to temperature burst kind of loading can also be analysed using this element, with great ease.

The numerical examples establish the spectrally formulated element as the most efficient tool for analysing wave propagation behavior. In many cases, a single element is sufficient to capture the wave propagation phenomena. It is shown that the element can capture the propagating shear mode quite effectively. Responses of the structure predicted by the element for different material variation models are almost identical, as found in the axial and the transverse velocity responses of cantilever beam. The stress history and stress pattern reveal dynamic stress transfer mechanism and stress smoothening effect of FGM. Further, study of the variation of maximum axial stress gradient and cut-off frequency with material property and the % FGM content reveals their qualitative dependence upon these parameters.

The next logical step is to consider the explicit coupling through the introduction of temperature as a degree of freedom. The thermal behavior dictated by Fourier heat conduction law can be coupled to the axial strains through the thermal constitutive law and resulting equation can be solved exactly. This will further enhance the insight into the behavior of FGM beam.

References

Chakraborty, A., Gopalakrishnan, S., Reddy, J.N., 2002. A new beam finite element for the analysis of functionally graded materials. International Journal of Mechanical Sciences, submitted for publication.

Christensen, R.M., 1979. Mechanics of Composite Materials. Wiley.

Doyle, J.F., 1988. A spectrally formulated finite element for longitudinal wave propagation. International Journal of Analytical and Experimental Modal Analysis 3, 1–5.

Doyle, J.F., 1999. Wave Propagation in Structures. Springer, NewYork.

Doyle, J.F., Farris, T.N., 1990a. A spectrally formulated finite element for flexural wave propagation in beams. International Journal of Analytical and Experimental Modal Analysis 5, 13–23.

Doyle, J.F., Farris, T.N., 1990b. A spectrally formulated finite element for wave propagation in 3-D frame structures. International Journal of Analytical and Experimental Modal Analysis, 223–237.

El-Abbasi, N., Meguid, S.A., 2000. Finite element modeling of the thermoelastic behavior of functionally graded plates and shells. International Journal of Computational Engineering Science 1 (1), 151–165.

Gong, S.W., Lam, K.Y., Reddy, J.N., 1999. The elastic response of functionally graded cylindrical shells to low-velocity impact. International Journal of Impact Engineering 22, 397–417.

Gopalakrishnan, S., Doyle, J.F., 1994. Wave propagation in connected waveguides of varying cross-section. Journal of Sound and Vibration 175 (3), 347–363.

Gopalakrishnan, S., Martin, M., Doyle, J.F., 1992. A matrix methodology for spectral analysis of wave propagation in multiple connected Timoshenko beam. Journal of Sound and Vibration 158, 11–24.

Han, X., Liu, G.R., Lam, K.Y., 2002a. Transient waves in plates of functionally graded materials. International Journal for Numerical Methods in Engineering 52, 851–865.

Han, X., Liu, G.R., Xi, Z.C., Lam, K.Y., 2002b. Characteristics of waves in a functionally graded cylinder. International Journal for Numerical Methods in Engineering 53, 653–676.

Jenkins, M.A., Traub, J.F., 1972. Zeros of a complex polynomial. Communications of the ACM 15, 97–99.

Jones, R.M., 1975. Mechanics of Composite Materials. Scripta, Washington, DC.

Liu, G.R., 1998. A step-by-step method of rule-of-mixture of fiber and particle-reinforced composite materials. Composite Structures 40, 313–322.

Liu, G.R., Han, X., Lam, K.Y., 1999. Stress wave in functionally gradient materials and its use for material characterization. Composite Part B 30, 383–394.

Liu, G.R., Tani, J., 1992. SH surface waves in functionally gradient piezoelectric material plates. Transactions of the Japan Society of Mechanical Engineers 58A (547), 504–507.

Liu, G.R., Tani, J., 1994. Surface waves in functionally gradient piezoelectric plates. ASME Journal of Vibration and Acoustics 116, 440–448.

Liu, G.R., Tani, J., Ohyoshi, T., 1991a. Lamb waves in a functionally gradient material plates and its transient response. Part 1: Theory, Part 2: Calculation results. Transactions of Japan Society of Mechanical Engineers 57A (535), 131–142.

Liu, G.R., Tani, J., Ohyoshi, T., Watanabe, K., 1991b. Transient waves in anisotropic laminated plates, part 1: Theory; Part 2: Applications. Journal of Vibration and Acoustics 113, 230–239.

Markworth, A.J., Ramesh, K.S., Parks Jr., W.P., 1995. Modelling Studies applied to functionally graded materials. Journal of Material Science 30, 2183–2193.

Martin, M., Gopalakrishnan, S., Doyle, J.F., 1994. Wave propagation in multiply connected deep waveguides. Journal of Sound and Vibration 174 (4), 521–538.

Müller, D.E., 1956. A method for solving algebraic equations using an automatic computer. Mathematical Tables and Aids to Computation 10, 208–215.

Ohyoshi, T., Sui, G.J., Miuro, K., 1996. Using of stacking model of the linearly inhomogeneous layers elements. Proceedings of the ASME Aerospace Division 52, 101–106.

Praveen, G.N., Reddy, J.N., 1998. Nonlinear transient thermoelastic analysis of functionally graded ceramic-metal plates. International Journal of Solids and Structures 35 (33), 4457–4476.

Reddy, J.N., 2000. Analysis of functionally graded plates. International Journal of Numerical Methods in Engineering 47, 663–684.

Reddy, J.N., Chin, C.D., 1998. Thermomechanical analysis of functionally graded cylinders and plates. Journal of Thermal Stresses 26 (1), 593–626.

Rizzi, S.A., Doyle, J.F., 1991. Force identification for impact of a layered system. Computational Aspects of Contact, Impact and Penetration, (BOOK–INVITED) Elmepress International, pp. 222–241.

Roy Mahapatra, D., Gopalakrishnan, S., Balachandran, B., 2001. Active feedback control of multiple waves in helicopter gear box support struts. Smart Materials and Structures 10, 1046–1058.

Roy Mahapatra, D., Gopalakrishnan, S., Shankar, T.S., 2000. Spectral-element-based solution for wave propagation analysis of multiply connected unsymmetric laminated composite beams. Journal of Sound and Vibration 237 (5), 819–836.

Suresh, S., Mortensen, A., 1998. Fundamentals of Functionally Graded Materials. IOM Communications Ltd, London.

Tsai, S.W., Hahn, H.T., 1980. Introduction to Composite Materials. Technomic.